J. Phys. Chem. **1987**, *91*, 719-724

Kinetics of the Gas-Phase Reaction $HOSO_2 + O_2 \rightarrow HO_2 + SO_3$

James F. Gleason, Amitabha Sinha, and Carleton J. Howard*

Aeronomy Laboratory, National Oceanic and Atmospheric Administration, Boulder, Colorado 80303, and Department of Chemistry and Biochemistry and Cooperative Institute for Research in Environmental Sciences, University of Colorado, Boulder, Boulder, Colorado 80303 (Received: July 29, 1986)

A flowing afterglow technique was adapted for use as a chemical ionization detector for kinetic measurments. Reactants and products from a radical flow tube reactor are injected into the flowing afterglow for detection via subsequent ion-molecule reactions. This system has been used to study the reaction $HOSO_2 + O_2 \rightarrow HO_2 + SO_3$, which is the second step in the homogeneous gas-phase oxidation of SO_2 to H_2SO_4. Both the $HOSO_2$ reactant and the SO_3 product were detected by using Cl^- as the chemical ionization reagent. The rate coefficient, which was determined by monitoring the loss of the $HOSO_2$ reactant, is $(4.37 \pm 0.66) \times 10^{-13}$ cm^3 molecule^{-1} s^{-1} at 298 K. This result supports earlier studies which claimed that odd hydrogen radicals (HO_x) are catalysts in the gas-phase oxidation of SO_2.

Introduction

The acid deposition problem has focused attention on the details of the mechanism for the oxidation of atmospheric sulfur dioxide to sulfuric acid.[1-3] Atmospheric sulfur dioxide is oxidized homogeneously in both the gas and liquid phases and probably heterogeneously on the surfaces of wet and dry aerosol particles. This study deals solely with the homogeneous gas-phase oxidation of SO_2.

The first step in the atmospheric gas-phase oxidation of SO_2 is generally accepted to be a termolecular reaction with the hydroxyl radical forming the bisulfite radical, $HOSO_2$:[3-5]

$$OH + SO_2 + M \rightarrow HOSO_2 + M \qquad (1)$$

This reaction has been well characterized in the laboratory by following the loss of OH in the presence of excess SO_2.[6,7] The identification of $HOSO_2$ and its subsequent atmospheric chemistry has been the subject of much speculation.[1-14]

A potential atmospheric observation of $HOSO_2$ has been reported by Arnold et al.[15] from in situ stratospheric ion composition measurements. They identified a series of negative ion clusters, $HSO_4^-(H_2SO_4)_nHSO_3$, $n = 1-3$, containing an $HOSO_2$ ligand. Using their composition measurements and a model of ion and neutral chemistry, they were able to infer $[HOSO_2] \approx 3 \times 10^5$ molecule cm^{-3} at 40.8 km.[16] It should be noted that their mass resolution was ±1 amu so they could not distinguish between SO_3 and $HOSO_2$. Another possible observation of this important radical comes from the work of Hashimoto et al.[17] who have reported a tentative identification of $HOSO_2$ in a solid Ar matrix using IR absorption spectroscopy.

By analogy to hydrocarbon chemistry, it was thought that the bisulfite radical would react with oxygen in an addition reaction forming the peroxybisulfate radical, $HOSO_2O_2$:[9]

$$HOSO_2 + O_2 + M \rightarrow HOSO_2O_2 + M \qquad (2)$$

The $HOSO_2O_2$ would eventually produce H_2SO_4 by an unknown mechanism. Proposed further reactions of $HOSO_2$ and $HOSO_2O_2$ include reactions with NO, NO_2, H_2O, hydrocarbons, and surface absorption.[8,11,14] Calvert et al.[8] reviewed the atmospheric chemistry of SO_2 and estimated that the only exothermic reactions of $HOSO_2$ of atmospheric interest were addition of O_2 and addition/complexation with H_2O. Hydrogen abstraction by O_2 to form HO_2 and SO_3 was estimated to be endothermic by 6 kcal mol^{-1}.[5]

$$HOSO_2 + O_2 \rightarrow HO_2 + SO_3 \qquad (3)$$

Whether the $HOSO_2 + O_2$ reaction proceeds by an addition mechanism or by a hydrogen abstraction has an important effect on the models used to describe atmospheric SO_2 oxidation. If reaction 2 were the dominant channel, each SO_2 oxidized removes at least one OH radical from the atmosphere; thus SO_2 terminates the HO_x chain. Since the source of OH, $O(^1D) + H_2O \rightarrow 2OH$, is weak, the atmosphere can become depleted of OH when the $[SO_2]$ is high, as in a power plant or smelter plume. If reaction 3 were the dominant channel, the HO_2 product may react with NO or O_3 to regenerate OH. In this case, SO_2 does not terminate the HO_x chain and the plume does not become depleted of HO_x. The atmospheric effects of these limiting cases will be explored in the Discussion section.

Recent work by Stockwell et al.[1] suggested that the hydrogen abstraction pathway may be the dominant channel for the reaction of bisulfite radicals with oxygen. Their experiments were carried out in a large steady-state photochemical reactor using long-path IR absorption to detect the stable reactants and products: CO, CO_2, SO_2, NO, NO_2, and H_2SO_4. A steady-state chain reaction was set up using reactions 4-6, where the rate of CO_2 formation

$$OH + CO \rightarrow CO_2 + H \qquad (4)$$

$$H + O_2 + M \rightarrow HO_2 + M \qquad (5)$$

$$HO_2 + NO \rightarrow OH + NO_2 \qquad (6)$$

was indicative of the steady-state OH concentration. When SO_2 was added to their reactor, they did not observe any change in the CO_2 formation rate, indicating that the OH loss due to reaction with SO_2 was not significant. They also reported the formation of sulfuric acid aerosol, indicating that SO_2 was being oxidized without terminating the OH chain reaction sequence. They postulated that reaction 3, not reaction 2, was occurring, and that OH was being regenerated in their system by reaction 6. They

---

* Author to whom correspondence should be addressed at NOAA R/E/AL-2, 325 Broadway, Boulder, CO 80303.

(1) Stockwell, W. R.; Calvert, J. G. *Atmos. Environ.* **1983**, *17*, 2231.
(2) Margitan, J. J. *J. Phys. Chem.* **1984**, *88*, 3314.
(3) Calvert, J. G.; Lazrus, A. L.; Kok, G. L.; Hiekes, B. G.; Walega, J. G.; Lind, J.; Cantrell, C. A. *Nature (London)* **1985**, *317*, 27.
(4) *Acid Deposition: Atmospheric Processes in Eastern North America*; National Research Council, National Academy Press: Washington, DC, 1983.
(5) Benson, S. W. *Chem. Rev.* **1978**, *78*, 23.
(6) Leu, M. T. *J. Phys. Chem.* **1982**, *86*, 4558.
(7) Wine, P. H.; Thompson, R. J.; Ravishankara, A. R.; Semmes, D. H.; Gump, C. A.; Torabi, A.; Nicovich, J. M. *J. Phys. Chem.* **1984**, *88*, 2095.
(8) Calvert, J. G.; Stockwell, W. R. *SO_2, NO and NO_2 Oxidation Mechanisms: Atmospheric Considerations*, Calvert, J. G., Ed.; Butterworth: Stoneham, MA, 1984; pp 1-62.
(9) Calvert, J. G.; McQuigg, R. D. *Int. J. Chem. Kinet. Symp.* **1975**, *1*, 113. Davis, D. D.; Klauber, G. *Int. J. Chem. Kinet. Symp.* **1975**, *1*, 543.
(10) Martin, D. L.; Jourdain, J. L.; LeBras, G. *J. Phys. Chem.* **1986**, *90*, 4143.
(11) Calvert, J. G.; Su, Fu; Bottenheim, J. W.; Strausz, O. P. *Atmos. Environ.* **1978**, *12*, 197.
(12) Meagher, J. F.; Olszyna, K. J.; Luria, M. *Atmos. Environ.* **1984**, *18*, 2095.
(13) Cox, R. A. *Int. J. Chem. Kinet. Symp. 1* **1975**, *1*, 379.
(14) Friend, J. P.; Barnes, R. A.; Vesta, R. M. *J. Phys. Chem.* **1980**, *84*, 2423.
(15) Arnold, F.; Viggiano, A. A.; Schlager, H. *Nature (London)* **1982**, *297*, 371.
(16) Arnold, F.; Qiu, S. *Planet. Space Sci.* **1984**, *32*, 169.
(17) Hashimoto, S.; Inoue, G.; Akimoto, H. *Chem. Phys. Lett.* **1984**, *107*, 198.

0022-3654/87/2091-0719$01.50/0 © 1987 American Chemical Society

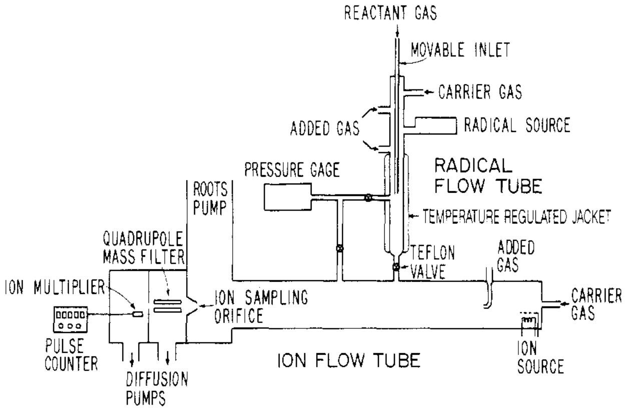

Figure 1. Experimental apparatus.

were unable to detect the reactive species $HOSO_2$, OH, HO_2, or SO_3 formed in their system.

With a flash photolysis apparatus, Margitan[2] tested the Stockwell and Calvert mechanism using a simpler chemical system and direct resonant fluorescence detection of OH. He was able to monitor the nonlinear decays of OH in the presence of SO_2, NO, and O_2, and by numerically modeling the reaction system, he deduced a rate constant for reaction 3 of $(4 \pm 2) \times 10^{-13}$ cm^3 molecule^{-1} s^{-1}. He was also unable to directly measure the reactive species, $HOSO_2$, SO_3, and HO_2. Additional evidence for the hydrogen abstraction channel was given by McKeen et al.[18] who modeled the stratospheric effects of the 1982 El Chichon volcano plume. If reaction 2 were the dominant channel, volcanic SO_2 would reduce the stratospheric [OH], and the plume should show the effects of this reduced OH concentration, e.g., increased [O_3]. Experimental observations of the El Chichon plume showed no [O_3] increase[18] and Burnett et al.[19] observed an increase in the total column [OH].

The findings of Arnold et al.[15] who reported $HOSO_2$ ligands in stable negative ions and the previous success of the flowing afterglow as a chemical ionization detector[20,21] inspired us to attempt a new scheme for $HOSO_2$ detection. Chemical ionization was the method of choice because previous attempts to detect $HOSO_2$ by conventional electron impact ionization had failed, possibly due to fragmentation of the parent molecule.[6,10]

Using a flowing afterglow apparatus as a chemical ionization mass spectrometer allows us to selectively ionize the species of interest by using the appropriate ion–molecule reaction. The principle is to select ionization reactions that cause little or no fragmentation of the parent molecule, allowing us to make an clear identification of the parent molecule. A typical example is reaction 7. This fast, $k_7 = 1.3 \times 10^{-10}$ cm^3 molecule^{-1} s^{-1},[23] charge-transfer

$$SF_6^- + NO_2 \rightarrow NO_2^- + SF_6 \tag{7}$$

reaction has been used to detect NO_2. The detection limit for NO_2, in the radical flow tube, is 3×10^8 molecule cm^{-3}.

Our objective was to detect gaseous $HOSO_2$ directly by using a soft ionization method and to employ this method to study the atmospheric reactions of $HOSO_2$.

Experimental Section

The experimental apparatus, shown in Figure 1, consists of two flow tubes, a horizontal ion flow tube (flowing afterglow) and a vertical radical flow tube. The details of the flowing afterglow technique can be found in the literature.[22] The flowing afterglow apparatus consists of a 1.5 m long × 7.62 cm i.d. stainless steel tube pumped by a 600 L s^{-1} pumping system. A large flow, 150–200 STP cm^3 s^{-1} (STP = 273 K, 1 atm), of helium carrier gas is introduced at one end of the tube, where electrons from a hot thorium oxide coated iridium filament ionize a small fraction of the gas by electron impact. Reagents can be added through side ports to make new ions via ion–molecule reactions. The pressure in the ion flow tube is measured about 10 cm from the downstream end with a differential capacitance manometer and is typically in the range of 0.2 to 0.6 Torr. At the downstream end of the tube, a small fraction of the gas is sampled through a 1.8-mm orifice. The ions are analyzed with a quadrupole mass filter and detected with a strip electron multiplier. The radical flow tube consists of a 1.5 m long × 2.54 cm i.d. Pyrex tube, with a 60-cm reaction zone. This zone is jacketed so that heated silicon oil or cooled ethanol can be circulated for temperature regulation. The contents of the neutral flow tube enter the flowing afterglow through a 1.6-cm o.d. Kel-F stopcock located approximately 55 cm upstream from the ion detection region. This valve allows us to maintain a significantly higher pressure in the radical flow tube, typically 2 to 8 Torr, than in the ion flow tube. The radical flow tube pressure is measured in the middle of the reaction zone by a differential capacitance manometer. The temperature is measured by inserting a thermocouple into the gas stream through the pressure port. All gas flows are measured with calibrated mass flowmeters.

The chemical ionization scheme for detecting $HOSO_2$ is shown in reactions 8–10. The ionization reagent, Cl$^-$, is produced by

$$e^- + CCl_4 \rightarrow Cl^- + CCl_3 \tag{8}$$

$$Cl^- + HOSO_2 \rightarrow SO_3^- + HCl \tag{9}$$

$$\Delta H^\circ_{acid}(HOSO_2) \approx DH^\circ(H\text{-}SO_3) + IP(H^\bullet) - EA(SO_3) \tag{10}$$

fast dissociative electron attachment to CCl_4, $k_8 = 4 \times 10^{-7}$ cm^3 molecule^{-1} s^{-1}.[24] $HOSO_2$ is ionized by a proton abstraction or a gas-phase acid–base reaction. The gas-phase acidity of $HOSO_2$ is not known, but it can be estimated by using a thermochemical cycle.[25] The $DH^\circ(H\text{-}SO_3) \approx 50$ kcal mol^{-1},[5] $IP(H^\bullet) = 313.6$ kcal mol^{-1},[25] and $EA(SO_3) \approx 39.2$ kcal mol^{-1};[26] therefore $\Delta H^\circ_{acid}(HOSO_2) \approx 324$ kcal mol^{-1}. A negative ion whose conjugate acid's gas-phase acidity is more positive than $HOSO_2$ can abstract a proton from $HOSO_2$. For HCl, $\Delta H^\circ_{acid} = 333.4$ kcal mol^{-1}; therefore it is exothermic for Cl$^-$ to abstract a proton from $HOSO_2$ and exothermic proton-transfer reactions are generally fast. The rate coefficient for reaction 9 has not been measured but for an analogous reaction, $Cl^- + HNO_3 \rightarrow HCl + NO_3^-$, $k = 2 \times 10^{-9}$ cm^3 molecule^{-1} s^{-1}.[27] The signal at m/e 80 is dependent on the simultaneous presence of H, NO_2, and SO_2 and conditions under which the OH + SO_2 adduct can be formed. If any of these are eliminated the signal disappears. Under these conditions, SO_3 cannot produce SO_3^- because the charge-transfer reaction is strongly endothermic and no free electrons or other ionizing reagents are available. The ion at m/e 80 is SO_3^-, produced by proton abstraction from $HOSO_2$, and the intensity of this signal is taken to be proportional to [$HOSO_2$].

The SO_3 is detected by a fast association reaction, $k_{11} = 7 \times 10^{-27}$ cm^6 molecule^{-2} s^{-1}.[28]

$$Cl^- + SO_3 + M \rightarrow (Cl\cdot SO_3)^- + M \tag{11}$$

Typical experimental conditions in the radical flow tube are as follows. Nitrogen carrier gas, 12–16 STP cm^3 s^{-1}, passes

---

(18) McKeen, S. A.; Liu, S. C.; Kiang, C. S. *J. Geophys. Res.* **1984**, *89*, D3, 4973.

(19) Burnett, C. R.; Burnett, E. B. *J. Geophys. Res.* **1984**, *89*, D3, 9603.

(20) Davidson, J. A.; Howard, C. J.; Schiff, H. I.; Fehsenfeld, F. C. *J. Chem. Phys.* **1979**, *70*, 1697.

(21) Viggiano, A. A.; Davidson, J. A.; Fehsenfeld, F. C.; Ferguson, E. E. *J. Chem. Phys.* **1981**, *74*, 6113.

(22) Ferguson, E. E.; Fehsenfeld, F. C.; Schmeltekopf, A. L. *Adv. At. Mol. Phys.* **1969**, *5*, 1.

(23) Streit, G. E. *J. Chem. Phys.* **1982**, *77*, 826. This measurement was confirmed in unpublished work done by J.F.G.

(24) Smith, D.; Adams, N. C.; Alge, E. *J. Phys. B* **1984**, *17*, 461.

(25) Bartmess, J. E.; McIver, R. T. In *Gas Phase Ion Chemistry*; Bowers, M. T., Ed.; Academic: New York, 1979; Vol. 2, Chapter 11.

(26) Janousek, B. K.; Brauman, J. I. In *Gas Phase Ion Chemistry*; Bowers, M. T., Ed.; Academic: New York, 1979; Vol. 2, Chapter 10.

(27) Albritton, D. L. *At. Data Nucl. Data Tables* **1978**, *22*, 1.

(28) Gleason, J. F.; Howard, C. J., manuscript in preparation.

through a cooled (193 K) 5A molecular sieve trap and enters at the top of the flow tube. The OH radicals, produced in a side arm reactor, are introduced 20 cm below the carrier gas inlet. The OH radicals are generated by the following reaction:

$$H + NO_2 \rightarrow OH + NO \qquad (12)$$

The H atoms are produced by passing a combination of (1–3) $\times$ 10^{-3} STP $cm^3\ s^{-1}$ of a 0.1% H_2 in He mixture and (3–6) STP $cm^3\ s^{-1}$ of He through a microwave discharge. These atoms are mixed with (1–3) $\times$ 10^{-4} STP $cm^3\ s^{-1}$ of NO_2. Reaction 12 is estimated to be 99.5% complete within the sidearm. The SO_2 is added to the flow tube about 1.5 cm downstream of the OH inlet. The O_2 is added through a 6.4-mm o.d. Pyrex moveable inlet. The SO_2 flow, 0.3–0.7 STP $cm^3\ s^{-1}$, and the inlet position are adjusted to allow reaction 1 to go to $\geq$99.5% completion before O_2 addition.

The initial OH concentration, $[OH]_0$, was determined by measuring the amount of NO_2 that was consumed by reaction 12. Assuming one OH was produced per NO_2 lost, we adjusted the experimental conditions so that reaction 12 was the only significant loss process for NO_2. The $[NO_2]$ was calculated by using the NO_2 flow rate. This flow rate was measured by the rate of pressure rise in a calibrated volume, the total gas flow, and flow tube pressure. NO_2 was detected by charge-transfer reaction 7. $S_{NO_2^-}$ is the NO_2^- signal normalized to the SF_6^- signal. The $[OH]_0$ was determined from the $S_{NO_2^-}$ with the microwave discharge turned on and off, and the $[NO_2]$ with the discharge off:

$$[OH]_0 = \frac{S_{NO_2^-(off)} - S_{NO_2^-(on)}}{S_{NO_2^-(off)}}[NO_2]_{off} \qquad (13)$$

Using this method, we can calculate $[OH]_0$. To minimize secondary chemistry, most of the experiments were done at $[OH]_0 \leq 2 \times 10^{11}$ molecule cm^{-3}. The $[OH]_0$ was varied from 1×10^{11} to 4×10^{11} molecule cm^{-3} to see if secondary chemistry was significant. The maximum $[HOSO_2]_0$ is equal to $[OH]_0$ and the $[HOSO_2]_0$ is usually less than $[OH]_0$ because some OH is lost to the reactor walls. Pseudo-first-order conditions, $[HOSO_2]_0 \leq 2 \times 10^{11}$ molecule cm^{-3} and $[O_2] \approx (8\text{–}200) \times 10^{12}$ were established for $HOSO_2$.

The walls of the OH source reactor were coated with H_3PO_4 to minimize wall losses and to assist deactivation of any vibrationally excited OH that was formed by reaction 10.[29] The walls of the reaction region in the radical flow tube were coated with halocarbon wax to minimize the wall loss of $HOSO_2$. It was necessary to condition the walls of the radical flow tube before each run. The radical flow tube was heated to 390 K, while 4 STP $cm^3\ s^{-1}$ of O_2 and 4×10^{-5} STP $cm^3\ s^{-1}$ of OH at 2 Torr were flowed through the radical flow tube for at least 3 h. Heating the tube to 340 K and flowing 3 STP $cm^3\ s^{-1}$ of N_2 at 1 torr overnight kept the radical flow tube clean and reduced the amount of conditioning required.

The differential capacitance manometer was calibrated with a precision water manometer. The accuracy of this method is ±0.5%. The mass flowmeters were calibrated with a wet-test meter for flows >2 STP $cm^3\ s^{-1}$ and by the rate of change in pressure in a calibrated volume for flows <2 STP $cm^3\ s^{-1}$. The accuracy of these methods is ±1%.

All gases, except where noted, were used without further purification steps.

In this study, all experiments were done at $T = 297 \pm 1$ K.

Results

The rate coefficient for reaction 3 was measured by two equivalent methods. In the first method, the moveable inlet position was fixed and the $[O_2]$ was varied. The advantage of this method was that the loss of the $HOSO_2$ on the moveable inlet wall was constant and therefore no correction for this effect was required, while the main disadvantage was that the absolute reaction time must be accurately known. In the second method, the $[O_2]$ was constant and the reaction distance and therefore the reaction time was varied by moving the inlet. A correction for the $HOSO_2$ loss on the moveable inlet wall was made, but the absolute reaction time was not required. The two methods are thus complementary.

TABLE I: Experimental Conditions for Fixed Inlet Method Measurement of k_3

O_2 compn	time, 10^{-3} s	$[SO_2]$, 10^{15} molecule cm^{-3}	press., Torr	range of k_3, 10^{-13} cm^3 molecule^{-1} s^{-1}	no. of expt
pure O_2	38–45	2.8–4.4	4.1–4.4	4.26–4.79	5
	60–65	5.7–6.3	4.3–4.4	4.04–4.79	5
20% O_2/N_2	33–39	1.7–1.9	4.0–4.1	4.37–4.83	3
	44–50	2.1–3.2	4.1	4.22–4.90	5
	50–77	1.02–2.78	4.1–8.3	4.22–4.87	7

For a flow tube reactor, the reaction time is calculated by dividing the reaction distance by the average flow velocity. In the radical flow tube, the flow velocity is not uniform in the region from the bottom of the flow tube through the Kel-F valve and into the ion-molecule flow tube. Therefore the absolute reaction time could not be calculated in the usual way. But the effective reaction time can be measured accurately by using a well-characterized reaction. The reaction chosen was OH + C_2H_6 because its rate coefficient, $k = 2.8 \times 10^{-13}$ cm^3 molecule^{-1} s^{-1},[30] is similar in magnitude to k_3, so that similar flow tube conditions could be used. The OH was detected by using SF_6^-, which charge transfers to OH to form OH^-:

$$SF_6^- + OH \rightarrow OH^- + SF_6 \qquad (14)$$

The ethane was added through the moveable inlet and the log (OH signal) vs. moveable inlet position was plotted. When several OH decays at different ethane concentrations were plotted on the same figure, the separate lines through the data points all intersect at a point corresponding to zero reaction time. This method was used to calibrate the reaction distance scale and therefore the absolute reaction time.

For the fixed inlet method, the reaction time was set between 22×10^{-3} and 65×10^{-3} s by using different O_2 inlet positions and flow velocities. The SO_3^- signal was normalized to the Cl^- signal to correct for the effect of fluctuations in the parent ion concentration. There was a small background signal at m/e 80 due to an unidentified ion and to the shoulder of an ion peak at m/e 83, probably SO_2F^- formed from impurities. This background signal was 2 to 5 times the instrument background and the SO_3^- signal was 200 to 1000 times the instrument background when no O_2 was present. Therefore, the SO_3^- signal decayed to a nonzero background at high $[O_2]$ or long reaction times. We used a nonlinear least-squares fitting routine[31] to solve for the rate coefficient, k_3, by fitting the data to the equation

$$\{SO_3^-/Cl^-\}_{O_2} = \{SO_3^-/Cl^-\}_0 \exp[-k_3[O_2]t] + C \qquad (15)$$

Nonlinear least-squares fitting was used because the background signal was very noisy and the best value for C could be found by using the fitting routine. Three parameters were fitted, $\{SO_3^-/Cl^-\}_0$, k_3, and C. The independent variable was $[O_2]$, the dependent variable was $\{SO_3^-/Cl^-\}_{O_2}$, and t was measured experimentally. Two of the parameters could be independently verified: $\{SO_3^-/Cl^-\}_0$, which is the normalized signal with no O_2 added and C which is the background signal at high $[O_2]$.

A typical decay plot is shown in Figure 2. The experimental conditions for the data measured in this way are summarized in Table I and the data are plotted in Figure 3 as k_3t vs. t. The slope of the line in Figure 3 gives the rate constant, $k_3 = (4.24 \pm 0.27) \times 10^{-13}$ cm^3 molecule^{-1} s^{-1}. The reported error limit is one standard deviation of the slope of the line.

---

(29) Spencer, J. E.; Glass, G. P. *Chem. Phys.* **1976**, *15*, 35.

(30) DeMore, W. B.; Margitan, J. J.; Molina, M. J.; Watson, R. T.; Golden, D. M.; Hampson, R. F.; Kurylo, M. J.; Howard, C. J.; Ravishankara, A. R. JPL Publication 85-37, Jet Propulsion Laboratory, California Institute of Technology, Pasadena, CA, 1985.

(31) Donaldson, J. R.; Tryon, P. V. *Natl. Bur. Stand.* (*U.S.*), *Tech. Note* **1983**, No. 1068-2.

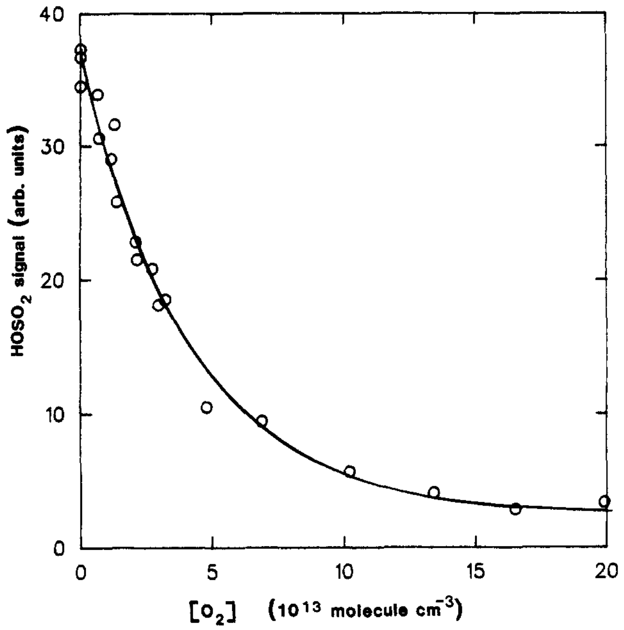

Figure 2. Fixed inlet decay of HOSO$_2$. The experimental conditions for the data shown are T = 297 K, flow velocity = 800 cm s^{-1}, pressure = 4 Torr. The experimental data are shown as the open circles and the fit to eq 15 is the solid line.

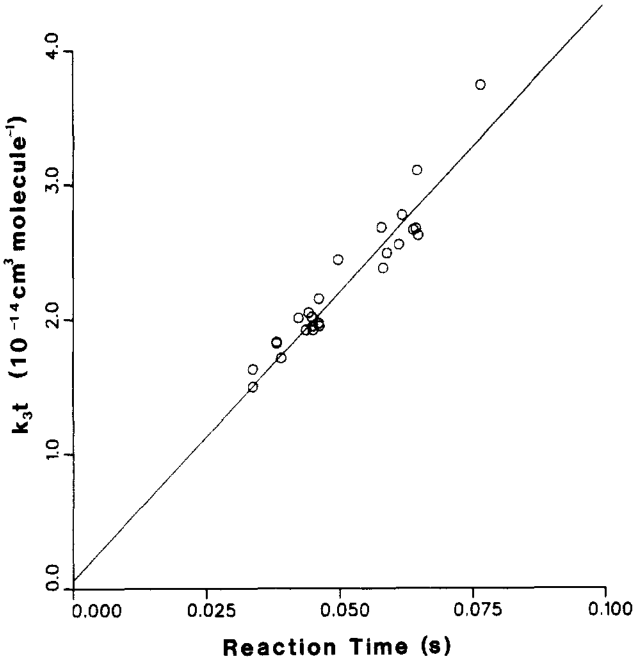

Figure 3. Plot of k_3t vs. t. The slope of the linear least-squares fit gives a rate coefficient of k_3 = (4.24 ± 0.27) × 10^{-13} cm^3 molecule^{-1} s^{-1}. The uncertainty is one standard deviation of the slope of the line and does not reflect any systematic errors. The data are summarized in Table I.

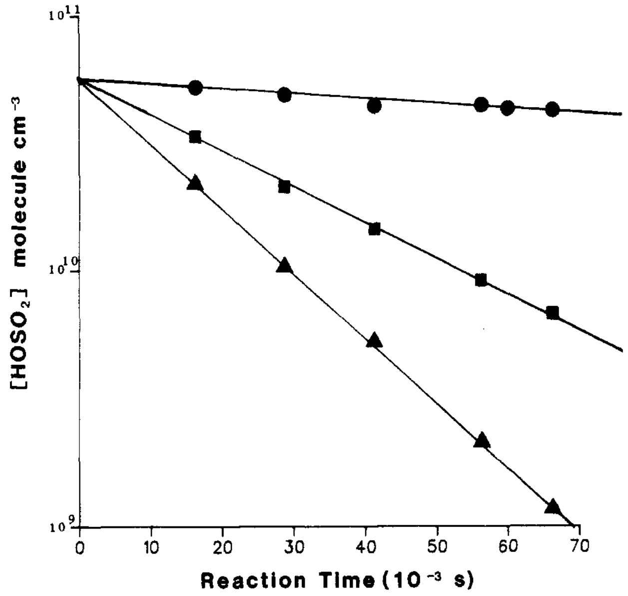

Figure 4. Moveable inlet decays of HOSO$_2$. The experimental conditions for the data shown are T = 296 K, flow velocity = 800 cm s^{-1}, pressure = 7 Torr. The O$_2$ concentrations in molecule cm^{-3} are [O$_2$] = 7.37 × 10^{12} for ●, [O$_2$] = 6.91 × 10^{13} for ■, [O$_2$] = 1.12 × 10^{14} for ▲.

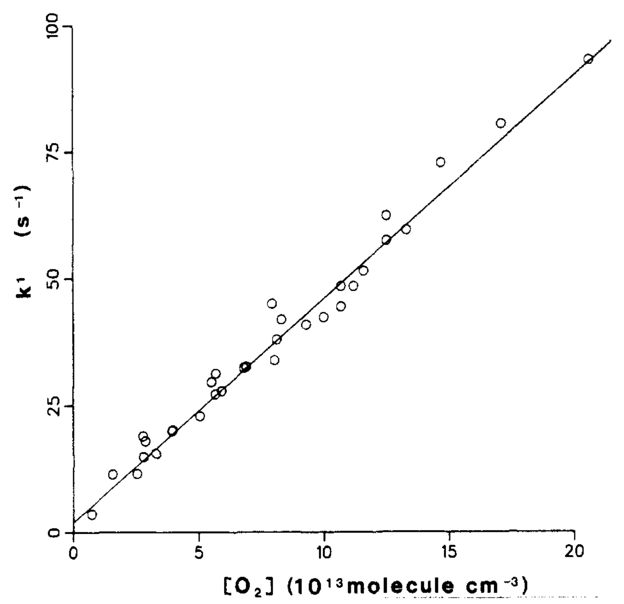

Figure 5. Plot of k^1 vs. [O$_2$]. The slope of the linear least-squares fit gives a rate coefficient of k_3 = (4.42 ± 0.12) × 10^{-13} cm^3 molecule^{-1} s^{-1}. The uncertainty is one standard deviation of the slope of the line and does not reflect any systematic errors. The data are summarized in Table II.

In the moveable inlet method, a blank run was made to measure the loss of HOSO$_2$ on the inlet surface before O$_2$ was added. The [HOSO$_2$] changed by a factor of ≈1.5 as the inlet was moved. A correction for this effect was applied to the data taken with the O$_2$ flow on. The log (corrected SO$_3^-$) was plotted as a function of time in Figure 4, where the slope of the lines are the pseudo-first-order rate coefficient for reaciton 3.

The initial data taken with this method showed an upward curvature at long reaction times and high [O$_2$]. Analysis of the NO$_2$ source gas showed that there was an excess of NO above the concentration produced by reaction 6. This NO reacted with the HO$_2$ product by reaction 10 to form OH which regenerated HOSO$_2$. Additional purification of the NO$_2$ by the addition of excess O$_2$ helped to reduce the NO levels but there was still some additional NO, possibly from the reduction of NO$_2$ on the surface of the stainless steel gas lines. To eliminate the problem of OH regeneration, an OH scavenger, C$_2$ClF$_3$, was added with the O$_2$ through the moveable inlet. The scavenger reacts rapidly with OH, k = 6 × 10^{-12} cm^3 molecule^{-1} s^{-1}, so that it cannot react with SO$_2$.[32] Enough scavenger, [C$_2$ClF$_3$] = 6 × 10^{14} molecule cm^{-3}, was added so that the OH removal rate by the scavenger was about 50 times faster than that by SO$_2$.

The data taken with the moveable inlet are summarized in Figure 5. The slope of the line gives the second-order rate constant, k_3 = (4.42 ± 0.12) × 10^{-13} cm^3 molecule^{-1} s^{-1}, which is in excellent agreement with the data taken with the first method. The reported error limit is one standard deviation of the slope of the line.

The experimental conditions are summarized in Table II. They were varied as follows: a factor of 4 in pressure, a factor of 4 in [SO$_2$], and a factor of 4 in [OH]$_0$. There were no systematic

---

[32] Howard, C. J.; Evenson, K. M. *Geophys. Res. Lett.* **1977**, *4*, 437.

TABLE II: Experimental Conditions for Moveable Inlet Method Measurement of k_3

$[OH]_0$, 10^{11} molecule cm^{-3}	$[SO_2]$, 10^{15} molecule cm^{-3}	press., Torr	range of k^1, s^{-1}	no. of expt
2	2.74	4	11.5–80.4	8
2	1.7	8	14.8–62.4	8
2	7.7	2	18–73	5
2	4.1	7	3.6–93	7
1–4	4.0	4	15.5–40	4

TABLE III: Comparison of Values for k_3

method[a]	k_3, cm^3 molecule^{-1} s^{-1}	comments	ref
DF-CIMS	$(4.37 \pm 0.66) \times 10^{-13}$	direct detection of $HOSO_2$ and SO_3	this work
FP-RF	$(4 \pm 2) \times 10^{-13}$	indirect study high pressure	2
DF-LMR	$(4.9 \pm 2.9) \times 10^{-13}$	detection of HO_2 product	34
DF-EPR	$(3.5 \pm 1) \times 10^{-13}$	indirect study low pressure	10

[a] DF = discharge flow, CIMS = chemical ionization mass spectrometry, FP = flash photolysis, RF = resonant fluorescence, LMR = laser magnetic resonance, EPR = electron paramagnetic resonance.

changes in the rate constant over the range of conditions tested.

From our data, we can put an upper limit on k_2. The pressure was varied from 2 to 8 Torr. Over this pressure range we did not see a significant change in k_3, $\Delta k_3 < 6.6 \times 10^{-14}$ cm^3 molecule^{-1} s^{-1}. This puts an upper limit on $k_2 \leq 3.4 \times 10^{-31}$ cm^6 molecule^{-2} s^{-1}, for $M = N_2$.

The presence of excess NO did not affect the data analysis in the first method because the fit to k_3 depends primarily on the initial points where the decay is the steepest. These points correspond to relatively low $[O_2]$ so that the OH regeneration was negligible.

The recommended value, $k_3 = (4.37 \pm 0.66) \times 10^{-13}$ cm^3 molecule^{-1} s^{-1}, is the weighted average of the two data sets. The weights were determined by the ratio of the standard deviation of the slope of the line in each data set, Figures 3 and 5. The value for the error limit of k_3 is approximately twice the precision of a single measurement. The precision of a single rate coefficient measurement at the 95% confidence level is about 8% as calculated by using the standard propagation of error analysis.[33] The following error estimates were used: gas flow rate, ±2%; flow tube pressure, ±1%; flow tube temperature, ±1%; flow tube radius, ±1%; and the decay plot slope, ±2%. The axial diffusion correction[33] in 4 Torr of N_2, using $D_{HOSO_2} = 150$ cm^2 s^{-1}, was calculated and found to be less than 1% and was not applied to the data.

Discussion

Previous studies involving HO_x–NO_x–SO_x systems have shown evidence for reaction 3. Cox[13] observed the production of NO_2 from photolyzed HONO in $NO/NO_2/SO_2$/air mixtures, indicating the generation of an oxidant, possibly $HOSO_4$ or HO_2. Leu,[6] in his study of reaction 1, observed OH reformation and nonlinear OH decay plots when $M = O_2$. The nonlinearity increased when additional NO was added. He did not speculate on the mechanism that regenerates OH when O_2 and NO are present.

The present results and three other measurements of k_3 are summarized in Table III. Bandow and Howard[34] used a laser magnetic resonance spectrometer to detect the HO_2 product of reaction 3 and to measure k_3 by monitoring the appearance of the HO_2 as a function of $[O_2]$. They find a $k_3 = (4.9 \pm 2.9) \times 10^{-13}$ cm^3 molecule^{-1} s^{-1}. Measuring a rate coefficient by monitoring the appearance of a product is often more difficult than monitoring the disappearance of a reactant because other reaction processes including wall losses must be accurately known. The $HOSO_2$ wall loss is difficult to measure without direct detection of the $HOSO_2$ and also has been found to vary over a period of several hours. Generally the wall loss rate increases with exposure to the $HOSO_2$ radical. This contributes to the large uncertainty in their measurement of k_3, although the value agrees well with this work.

This study supports the earlier work by Margitan,[2] $k_3 = (4 \pm 2) \times 10^{-13}$ cm^3 molecule^{-1} s^{-1}. The agreement between these two studies is excellent considering the different experimental techniques and conditions. Ours is a direct measurement and Margitan's is an indirect one that required a numerical simulation of a reaction mechanism with five known rate coefficients and two unknown rate coefficients, k_3 and $k(HOSO_2 + NO)$. The agreement between our study at 4 Torr and Margitan's at 200 Torr suggests that the termolecular component of the $HOSO_2 + O_2$, reaction 2, is quite slow. Margitan's work at 200 Torr can used to put an upper limit on k_2. Using his error limits for k_3 yields $k_2 \leq \Delta k_3 = 2 \times 10^{-13}$ cm^3 molecule^{-1} s^{-1} at 200 Torr, which gives an upper limit for $k_2 \leq 3 \times 10^{-32}$ cm^6 molecule^{-2} s^{-1}. Schmidt et al.[35] have repeated Margitan's experiment at 760 Torr. Their numerical simulations, using Margitan's value for k_3, show that greater than 90% of the OH is regenerated in the SO_2 catalytic oxidation. This puts an even smaller upper limit on k_2: $k_2 \leq 4 \times 10^{-14}$ cm^3 molecule^{-1} s^{-1} at 760 Torr which gives an upper limit of $k_2 \leq 2 \times 10^{-33}$ cm^6 molecule^{-2} s^{-1}, for the effective termolecular rate coefficient.

Martin et al.[10] have recently completed an indirect low-pressure flow tube measurement of k_3. They used electron paramagnetic resonance (EPR) to monitor the nonlinear decay of OH in the presence of SO_2, O_2, and NO. Their numerical simulations required nine known reaction rate coefficients and three unknown reaction rate coefficients, k_3, $k(HOSO_2 + NO)$, and $k(HOSO_2 + \text{wall})$. Their value of $k_3 = (3.5 \pm 1) \times 10^{-13}$ cm^3 molecule^{-1} s^{-1} is in good agreement with the other measurements.

One expects the atmospheric $[HOSO_2]$ to be quite small because of its rapid reaction with O_2. Near the earth's surface, the lifetime of $HOSO_2$ is only 5×10^{-7} s. In light of this development, Schlager and Arnold[36] have recently reinterpreted their earlier measurements. They observed in the laboratory than an ion of mass 80, presumably SO_3^- and clusters containing this mass, are produced in a drift field by the fragmentation of $HSO_4^-(H_2SO_4)_n$, $n = 1, 2$. Similar drift fields were used to sample the stratospheric ions, previously identified as containing $HOSO_2$. They now propose that the clusters reported by Arnold et al.[15,16] were artifacts produced by fragmentation during the sampling process and that these ions cannot be used to deduce the SO_3 or $HOSO_2$ concentrations in the stratosphere.

As briefly mentioned in the Introduction, the choice of reaction 2 or reaction 3 as the dominant path leads to two quite different mechanisms for atmospheric SO_2 oxidation. How the choice of oxidation mechanism affects the predictions of atmospheric models has been explored by two studies.[37,38] In the first, Samson[37] has examined the relationship between SO_2 emission and SO_4^{2-} deposition. This type of analysis is very important for designing and implementing control strategies for SO_2 emissions. When reaction 2 was used in this atmospheric model, SO_2 had the effect of acting as a sink for HO_x radicals. SO_2 terminated the HO_x chain, and the OH oxidant was depleted. The SO_2 oxidation rate was limited by the OH production rate and not by the amount of SO_2 present. Therefore, the relationship between SO_2 emission and SO_4^{2-} deposition was very nonlinear. When reaction 3 was put into this model, SO_2 acted as a chain carrier and OH catalytically oxidized SO_2. The OH oxidant was not depleted by SO_2 and the rela-

---

(33) Howard, C. J. *J. Phys. Chem.* **1979**, *83*, 3.

(34) Bandow, H.; Howard, C. J. *Atmos. Chem.*, manuscript in preparation.

(35) Schmidt, V.; Zhu, G. Y.; Becker, K. H.; Fink, E. H. *Ber. Bunsenges. Phys. Chem.* **1985**, *89*, 321.

(36) Schlager, H.; Arnold, F. *Planet. Space Sci.* **1986**, *34*, 245.

(37) Samson, P. J. "On the Linearity of Sulfur Dioxide to Sulfate Conversion in Regional-Scale Models", Office of Technology Assessment, U.S. Congress, OTA Contractor Report, June 1984, and "Regional Acid Deposition: Models and Physical Processes"; NCAR Technical Note: NCAR/TN-214+STR, National Center for Atmospheric Research, Boulder, CO.

(38) Stockwell, W. R. *Atm. Environ.* **1986**, *20*, 1615.

tionship between SO$_2$ emission and SO$_4^{2-}$ deposition becomes more nearly linear.

The effects of chain termination vs. chain propagation were explored in more detail by Stockwell[38,39] using the National Center for Atmospheric Research's Regional Acid Deposition Model (RADM) gas-phase chemistry mechanism. The Samson simulation used extremely simple chemistry, only 19 reactions and very few of the reactions which compete for OH and HO$_2$. The RADM model is considerably more complex, employing 80 reactions and most of the organic and inorganic chemistry that competes for and generates OH and HO$_2$. The RADM model simulations were made for a 24-h period, from sunrise to sunrise. The concentrations of the various species of atmospheric interest have been compared for SO$_2$ oxidation with both the HO$_x$ propagation and the HO$_x$ termination mechanisms. The RADM simulation conditions are SO$_2$, 60 ppbv; NO$_x$, 100 pptv to 1 ppmv; hydrocarbons, 1 ppbv to 10 ppmv; temperature, 298 K; solar irradiance, June day at 40° N.

The RADM results show that the choice of mechanism has the greatest effect in clean air conditions, NO$_x$(NO + NO$_2$) $<$ 10 ppbv (ppbv = parts per billion by volume), and hydrocarbons (HC) $<$ 75 ppbv. Under these conditions, or in a high [SO$_2$], low [NO$_x$] plume, the propagation mechanism produces significantly more H$_2$SO$_4$ and orders of magnitude more H$_2$O$_2$.[39] The latter is an important condensed phase SO$_2$ oxidant. As the initial conditions move to higher levels of NO$_x$ and hydrocarbons, the differences between the two mechanisms become less pronounced, to the point when the air quality reaches urban levels, NO$_x$ $\leq$ 100 ppbv, HC $\leq$ 750 ppbv; there are not significant differences between the mechanisms.

We have additional studies in progress to determine the temperature dependence of k_3 and to measure the yield of SO$_3$.

Acknowledgment. This work was supported by NOAA as part of the National Acid Precipitation Assessment Program. We thank our colleagues, D. W. Fahey and F. C. Fehsenfeld, for numerous helpful discussions concerning the flowing afterglow apparatus and W. R. Stockwell of NCAR for helpful advice and providing the results and implications of the RADM model calculations. We also thank D.W.F. for his critical reading of this manuscript.

Registry No. HOSO$_2$, 104267-22-3; O$_2$, 7782-44-7.

(39) Stockwell, W. R., submitted to *J. Geophys. Res.*

Kinetics of Proton Transfer in (H$_3$CH$\cdot\cdot$CH$_3$)$^-$

Steve Scheiner*[†] **and Zdzisław Latajka**[‡]

Department of Chemistry & Biochemistry, Southern Illinois University, Carbondale, Illinois 62901

(Received: August 11, 1986)

The rates of proton transfer in (H$_3$CH$\cdot\cdot$CH$_3$)$^-$ and its fully deuteriated derivative are calculated by RRKM theory, including contributions from tunneling for energies below the barrier. These results are compared with rates calculated by canonical transition-state theory, incorporating two different tunneling corrections. For temperatures in excess of ca. 500 K, tunneling may be neglected, with all procedures converging on similar transfer rates. However, tunneling plays a progressively larger role as the temperature is lowered, speeding up the transfer by a factor of 30 at 300 K, and completely dominating the reaction below 200 K. The deuterium isotope effect is quite large (10^5) at 0 K, remains fairly constant as the temperature is raised to 50 K, and then drops precipitously from 50 to 500 K, after which it levels off to a high temperature limit of 1.12. The curvature exhibited by an Arrhenius plot below 500 K is unambiguously assigned to tunneling. Adjustment of transition-state theory for tunneling by the Wigner correction is incapable of reproducing the above behavior in the temperature regime where tunneling is important. However, an alternate correction, involving a summation of transmission coefficients, provides an improved recipe for incorporating tunneling into transition-state theory.

Intermolecular proton transfer in the gas phase may, in general, be partitioned into three sequential steps:

$$AH + B^- \xrightarrow[\text{association}]{} (AH\cdot\cdot B)^- \xrightarrow[\text{proton transfer}]{} (A\cdot\cdot HB)^- \xrightarrow[\text{dissociation}]{} A^- + HB \quad (1)$$

In those cases where the overall reaction is appreciably exothermic, the entire process has typically been found to proceed at or near unit efficiency with a rate limited only by the rate of diffusion together of the reactants in the association step.[1-3] Because of this, it has not been possible to extract much information about the proton-transfer step except for a lower limit to its rate. A principal factor contributing to the very fast proton-transfer rate has been the small energy barrier for those cases investigated. For typical H-bonded systems in which the transfer takes place between O or N atoms, the barrier is generally less than 5 kcal/mol, many times smaller than the energy available from the highly exothermic association step preceding it.[1-8] In fact, in many cases there is no barrier at all since the proton-transfer potential contains only a single minimum,[9] corresponding to (AH$\cdot\cdot$B)$^-$, (A$\cdot\cdot$HB)$^-$ or some intermediate structure such as (A$\cdot\cdot$H$\cdot\cdot$B)$^-$.

[†] Recipient of NIH Research Career Development Award.

[‡] Current address: Institute of Chemistry, University of Wrocław, Wrocław, Poland.

(1) Bohme, D. K.; Mackay, G. I.; Tanner, S. D. *J. Am. Chem. Soc.* **1979**, *101*, 3724. Dheandhanoo, S.; Forte, L.; Fox, A.; Bohme, D. K. *Can. J. Chem.* **1986**, *64*, 641. Bohme, D. K.; Mackay G. I.; Schiff, H. I. *J. Chem. Phys.* **1980**, *73*, 4976. Smith, D.; Adams, N. G.; Henchman, M. J. Ibid. **1980**, *72*, 4951. Henchman, M.; Hierl, P. M.; Paulson, J. F. *J. Am. Chem. Soc.* **1985**, *107*, 2812. Ausloos, P.; Lias, S. G. Ibid. **1981**, *103*, 3641. Bohme, D. K.; Rakshif, A. B.; Mackay, G. I. Ibid. **1982**, *104*, 1100.

(2) Squires, R. R.; Bierbaum, V. M.; Grabowski, J. J.; DePuy, C. H. *J. Am. Chem. Soc.* **1983**, *105*, 5185.

(3) Farneth, W. E.; Brauman, J. I. *J. Am. Chem. Soc.* **1976**, *98*, 7891. Moylan, C. R.; Brauman, J. I. *J. Phys. Chem.* **1984**, *88*, 3175. *Annu. Rev. Phys. Chem.* **1983**, *34*, 187.

(4) Huppert, D.; Bondybey, V. E.; Rentzepis, P. M. *J. Phys. Chem.* **1985**, *89*, 5811. Bondybey, V. E.; Haddon, R. C.; English, J. H. *J. Chem. Phys.* **1984**, *80*, 5432. Bondybey, V. E.; Haddon, R. C.; Rentzepis, P. M. *J. Am. Chem. Soc.* **1984**, *106*, 5969. Rossetti, R.; Rayford, R.; Haddon, R. C.; Brus, L. E. Ibid. **1981**, *103*, 4303.

(5) Strandjord, A. J. G.; Barbara, P. F. *Chem. Phys. Lett.* **1983**, *98*, 21. *J. Phys. Chem.* **1986**, *89*, 2355. Strandjord, A. J. G.; Smith, D. E.; Barbara, P. F. Ibid. **1985**, *89*, 2362.

(6) Woolfe, G. J.; Thistlethwaite, P. J. *J. Am. Chem. Soc.* **1981**, *103*, 6916.

(7) McMorrow, D.; Dzugan, T. P.; Aartsma, T. J. *Chem. Phys. Lett.* **1984**, *103*, 492. McMorrow, D.; Kasha, M. *J. Phys. Chem.* **1984**, *88*, 2235. Chou, P.; Aartsma, P. J. Ibid. **1986**, *90*, 721. Chou, P.; McMorrow, D.; Aartsma, T. J.; Kasha, M. Ibid. **1984**, *88*, 4596.

0022-3654/87/2091-0724$01.50/0